Journal of Controlled Release 338 (2021) 137–148

Contents lists available at ScienceDirect

Journal of Controlled Release

journal homepage: www.elsevier.com/locate/jconrel

M01 as a novel drug enhancer for specifically targeting the blood-brain barrier.

Olga Breitkreuz-Korff [a], Christian Tscheik [a], Giovanna Del Vecchio [a], Sophie Dithmer [a], Wolfgang Walther [b], Andrea Orthmann [c], Hartwig Wolburg [d], Reiner F. Haseloff [a], Leif Schröder [e], Ingolf E. Blasig [a,*], Lars Winkler [a,c,*]

[a] Leibniz-Forschungsinstitut für Molekulare Pharmakologie, Berlin, Germany
[b] Experimental and Clinical Research Center, Charité Universitätsmedizin, Berlin, Germany
[c] Experimentelle Pharmakologie und Onkologie Berlin-Buch GmbH, Germany
[d] Universität Tübingen, Germany
[e] German Cancer Research Center (DKFZ), Heidelberg, Germany

ARTICLE INFO

Keywords:
Drug delivery
Claudin
Tight junctions
Blood-brain barrier
Small molecule
Permeability enhancer
beta-catenin
Glioblastoma

ABSTRACT

Drug delivery to the brain is limited for most pharmaceuticals by the blood-brain barrier (BBB) where claudin-5 dominates the paraendothelial tightening. For circumventing the BBB, we identified the compound M01 as a claudin-5 interaction inhibitor. M01 causes transient permeabilisation of the BBB depending on the concentration of small molecules in different cell culture models within 3 to 48 h. In mice, brain uptake of fluorescein peaked within the first 3 h after M01 injection and normalised within 48 h. Compared to the cytostatic paclitaxel alone, M01 improved delivery of paclitaxel to mouse brain and reduced orthotopic glioblastoma growth. Results on interactions of M01 with claudin-5 were incorporated into a binding model which suggests association of its aromatic parts with highly conserved residues of the extracellular domain of claudin-5 and adjacent transmembrane segments. Our results indicate the following mode of action: M01 preferentially binds to the extracellular claudin-5 domain, which weakens *trans*-interactions between adhering cells. Further decrease in membranous claudin-5 levels due to internalization and transcriptional downregulation enables the paracellular passage of small molecules. In summary, the first small molecule is introduced here as a drug enhancer, which specifically permeabilises the BBB for a sufficient interval for allowing neuropharmaceuticals to enter the brain.

1. Introduction

Tight junctions (TJs) are one of the main restrictors for the permeability of solutes across epithelial and endothelial cell barriers. They consist of transmembrane proteins, in particular claudins [1] and TJ-associated MARVEL proteins, such as occludin [2]. In addition, cytosolic TJ-plaque proteins (e.g., Zonula occludens protein-1, ZO-1) are associated with the TJs. Within TJs, claudins have a superior role in sealing the paracellular space against water soluble molecules and ions [3]. Tissue compartmentation and homeostasis is thus a consequence of the spatial restriction. However, the tightening activity of the 25 members of the claudin family [1,4] differs considerably, and permeability properties of a cell layer are largely determined by the tissue-specific claudin expression pattern [1].

The blood-brain barrier (BBB) is one of the most restrictive cell barriers. Brain capillary endothelial cells form the BBB under the influence of surrounding structures and constitute a prerequisite for the homeostasis of the central nervous system. In these endothelial cells, the paracellularly tightening claudin-5 is the functionally dominating claudin [5,6]. The deficiency of claudin-5 is lethal for new-born mice [7]. Knockout and siRNA revealed that loss of claudin-5 from brain microvascular endothelial cells leads to a size-selective BBB opening for molecules ≤800 Da [7,8] - the molecular range of 98% of all pharmaceuticals [9,10]. While protecting the brain against harmful substances, the claudin-5-mediated BBB tightening is a major obstacle for the paraendothelial delivery of hydrophilic drugs [11].

Claudins are composed of four transmembrane helices [12], an extracellular oligomerisation domain [12,13], intracellular loop, cytosolic N- and C-terminus [3]. Their paracellular tightening function is mediated by the extracellular domain [14,15] via direct intercellular

* Corresponding authors.
E-mail addresses: ibasig@berlincures.com (I.E. Blasig), lars.winkler@live.de (L. Winkler).

https://doi.org/10.1016/j.jconrel.2021.08.014
Received 21 March 2020; Received in revised form 5 August 2021; Accepted 8 August 2021
Available online 10 August 2021

association between claudins from adjacent cells, called *trans*-interaction [16]. Consequently, targeting claudin-5 oligomerisation is a promising strategy for a specific and size-selective permeabilisation of the BBB to increase the uptake of small hydrophilic drugs to the brain.

Procedures to permeabilise the BBB, which are in clinical use (hyperosmolar mannitol) or in clinical testing (e.g., ultrasound, nanoparticles), are not target-oriented. Moreover, the latter are accompanied by serious side-effects, problems with dosing or with reproducibility [17]. Several other small molecules, such as Labradimal (also referred to as RMP-7 or Cereport®), AT1001 (synonym: larazotide acetate) or PN159 have been tested for their ability of transient opening of the BBB. Despite encouraging results in cellular and animal models, their clinical use as permeation enhancers has been abandoned [18]. This also refers to the application of short chain alkylglycerols for BBB opening [19]. Nanomedical approaches raised great expectations with respect to their use as permeability enhancers; several types of nanoparticles providing BBB drug transport have been or are currently being investigated in clinical trials for their efficacy in brain tumour treatment, in particular glioblastoma multiforme [20]. Specific peptidomimetics derived from claudins expressed at the BBB are target-oriented [21,22]. It has been shown that treatment with synthetic peptides from the extracellular domain of claudin-5 permeabilises cell culture models of the BBB as well as the murine BBB in vivo and improves the permeability of cytostatics such as doxorubicin [22]. However, proper generation and handling of peptide drugs is expensive, and degradation and rapid elimination limit the bioavailability of short-chain peptides.

Consequently, the aim of this study was to identify agents that fulfil the prerequisites for the development of pharmaceuticals [9,23]. Candidate molecules were characterized as preferentially associating to claudin-5 and were proven to permeabilise the BBB transiently and moderately to avoid side effects. This approach was successfully exploited for improved delivery of cytostatics to reduce brain tumour growth.

2. Material and methods

2.1. Drug enhancers

Drug enhancers investigated to modulate claudin-5 tissue barriers are depicted in Fig. 1A. M01 and derivatives were purchased from SIA Enamine Riga, Latvia, for substance screening experiments, cell culture experiments with Madin-Darby canine kidney (MDCK-II) or human embryonic kidney (HEK)-293 cells, and all experiments with M01A and —B. Experiments with bEnd.3 and all animal experiments were performed with M01, 2-[5-(*p*-Methoxyphenyl)-3-phenyl-4,5-dihydro-1H-pyrazol-1-yl]-2-oxoethyl 1-ethyl-7-methyl-4-oxo-1,8-diaza-3-naphthoate], synthesized by ASCA GmbH (Berlin, Germany). Properties of M01 ($C_{30}H_{28}N_4O_5$) are given Fig. 1A. The purity, proven by mass spectrometry, was >95%.

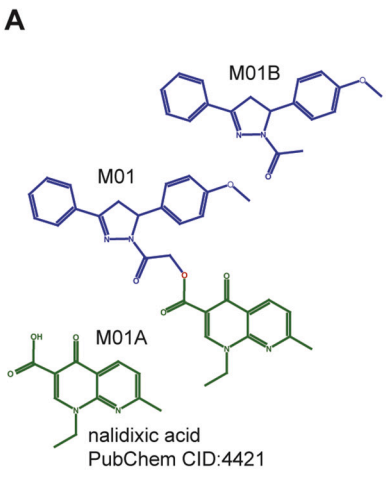

physicochemical properties table

	M01	M01A	M01B
atoms	67	28	40
mass (Da)	524.6	232.2	294.3
cLogP	2.792	1.024	3.076
HB-accep.	7	5	3
HB-donors	0	1	0
RotBonds	8	2	3
LogBB	0	0	0

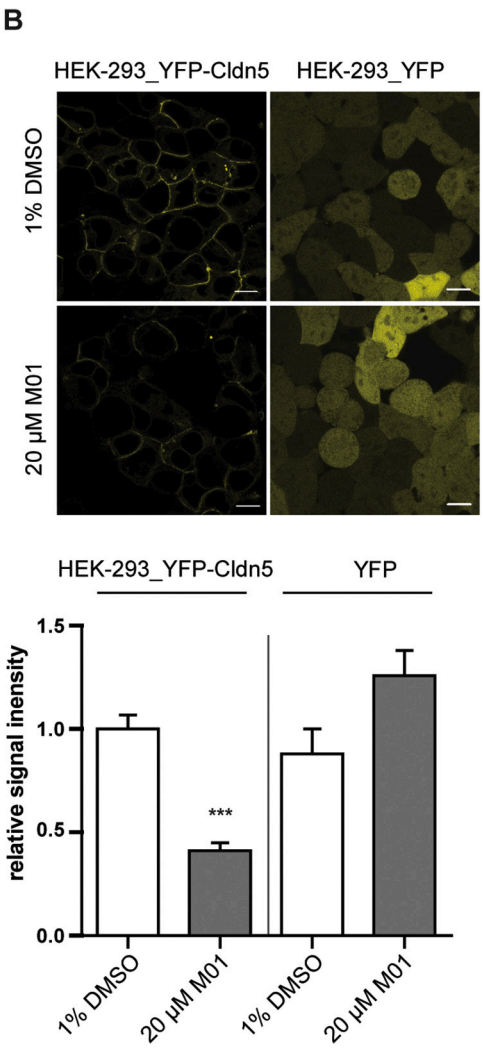

Fig. 1. M01, a small molecule affecting the tight junction protein claudin-5. M01 was identified in a screening approach (supplementary Materials and Methods). A) Structure and physicochemical properties of M01 and its derivatives M01A and M01B. B) Yellow fluorescence protein (YFP)-Cldn5 but not YFP expressing human embryonic kidney (HEK-293) cells showed reduced YFP-fluorescence after overnight treatment with 20 µM M01 in live cell imaging. Scale bar, 10 µm. The fluorescence intensity was quantified and normalised to DMSO treated control conditions (bar chart, bottom). Data presented as mean ± SEM, $n \geq 16$ images, Kruskal-Wallis-test followed by Dunn's multiple comparison test. ***, $p < 0.001$. (For interpretation of the references to colour in this figure legend, the reader is referred to the web version of this article.)

2.2. Cell culture

HEK-293 (passage 22) and MDCK-II cells (passage 34) were maintained in Dulbecco's modified Eagle's medium (DMEM; Life Technologies, Darmstadt, Germany), including 10% foetal calf serum (FCS; Life Technologies), 100 units/ml penicillin, 100 mg/ml streptomycin (Biochrom, Berlin, Germany) at 37 °C and 10% CO_2 [21]. The murine brain endothelial cell line bEND.3 [22] (a gift of Anuska Andjelkovic, University of Michigan; passages 20–28) was cultivated under the same conditions but with 4.5 g/l glucose DMEM (Thermo Fisher Scientific, Darmstadt, Germany). HEK-293 (ACC 305) and MDCK-II cells (ACC 169) were obtained from the German Collection of Microorganisms and Cell Cultures GmbH (Braunschweig, Germany). All claudin-transfected cells were used as stably expressing cell lines (HEK-293: EYFP-cldn-1, −3, −4, −5, YFP_{STOP}, and cldn-1-, cldn-2-, cldn-3-, cldn-4- and cldn-5-EYFP; MDCK-II: flag-cldn-5). Plasmids are listed in Supplementary Table 1. Stable cell lines were generated by transfection of 90% confluent cells on poly-L-lysine hydrobromide (20 μg/ml in Dulbecco's phosphate buffered saline (DPBS; Sigma-Aldrich, Taufkirchen, Germany) coated 6-well plates (TPP, Trasadingen, Germany) with 2 μg plasmid DNA and 10 μl polyethyleneimine (PEI, #23966–1, Polyscience Europe GmbH, Eppelheim, Germany) mixed with 250 μl Opti-MEM (Biochrom). Next day, the transfection mix was exchanged against culture medium with 0.5 μg/ml geneticin (Biochrom). FACS (FACSaria, Becton Dickinson, Heidelberg, Germany) was performed to enrich YFP-expressing cells. Harvested claudin expressing cells were cultivated and aliquots frozen in liquid nitrogen until use.

2.3. Cytotoxicity

Confluent cells (48-well plates coated with rat-tail collagen, Roche Diagnostics, Mannheim, Germany) were incubated with test compounds in complete medium without phenol red for 16 h. Cells were washed, and 200 μl MTT (3-(4,5-dimethylthiazol-2-yl)-2,5-diphenyltetrazoliumbromide; 0.5 g/ml, Sigma–Aldrich) was added to each well [22]. After 3 h, cells were washed and 200 μl of extraction solution per well was added (5% Triton X-100, 95% isopropanol). After 15 min vortexing (800 U/min), the signal intensity was determined (at 570 nm) using a plate reader (Safire, Tecan Infinite M1000 Pro; Tecan, Maennedorf, Switzerland) to calculate cell viability.

2.4. Microscale thermophoresis

Lysates were obtained from nearly confluent stably transfected HEK-293 claudin-YFP [24] or YFP alone expressing cells as negative control: cells were washed (2× PBS), scraped off, and centrifuged (10 min, 250 ×*g*). Pellets were resuspended in lysis buffer (20 mM Tris/HCl, pH 7.5, 100 mM NaCl, 1 mM $MgCl_2$, 5% glycerol, 5 units benzonase containing protease inhibitors (Roche)), pressed 5× through a 25-G needle, and centrifuged (10 min, 10,000 ×*g*, 4 °C) [25]. M01 was added in a defined amount as titration series (15 dilutions) in PBS to cell lysates containing fluorescently labelled claudins 1 to 5. After incubation (1 h, 22 °C), samples were loaded into standard treated capillaries, and the fluorescence was measured with Monolith NT.115 (light-emitting diode power 50%, infrared laser power 80%, and laser on time 35 s). The evaluation was performed with NT Analysis software 1.2.229 (NanoTemper, Munich, Germany), and binding was characterized by the dissociation constant (K_d). Determination was accomplished using saturation curves obtained at equilibrium conditions.

2.5. Transcellular electrical resistance (TER), impedance and permeation measurements

Resistance of bEND.3 cell monolayers seeded in 8-well electrode arrays (Electric Cell-Substrate Impedance System; model 1600R, Applied Biophysics, Troy, NY) were measured at 4 kHz and used to evaluate the impedance. At plateau values, cells were treated with the compounds tested. MDCK-II or MDCK-II-flag-Cldn5 were grown on rat-tail collagen–coated transwell filter inserts (10 mm diameter, 0.4 μm pore size, Millicell-CM; Millipore, Eschborn, Germany). TER was measured with an EVOM voltohmmeter (WPI, Sarasota, USA) and calculated in $\Omega \cdot cm^2$. Permeation was determined using 457-Da lucifer yellow (LY, Sigma–Aldrich) that was added luminally. LY (0.05 mg/ml) was dissolved in permeation buffer: Hank's buffered salt solution Ca^{2+}/Mg^{2+} ($HBSS^{+/+}$, Thermo Fisher), 5% FCS, and 10 mM HEPES (4-(2-hydroxyethyl)-1-piperazineethanesulfonic acid; PAA Laboratories, Pasching, Austria). Fluorescence of LY was measured with a microplate reader (Tecan) and the apparent permeability coefficient (P_{app}) was calculated by the following equation: $P_{app} = dQ/dt \cdot (1/A \cdot C_0 \cdot 60)$ in cm/s; dQ/dt is the permeability of the tracer (mg/min), A is the surface area of the filter (cm^2), C_0 is the concentration of the tracer in the apical compartment (mg/min) [21].

2.6. Quantitative real-time polymerase chain reaction (qRT-PCR)

RNA was extracted using GeneMATRIX Universal RNA Purification Kit (EURx, Gdansk, Poland). The cDNA was synthesized with the Maxima First Strand cDNA Syntheses Kit (Thermo Fisher Scientific). qRT-PCR was performed with StepOnePlus RT-PCR system (48/96well, Life Technologies) using Luminaris Color HiGreen high ROX qPCRMasterMix (Thermo Fisher Scientific) according to the manufacturer's recommendations. Primer pairs for qRT-PCR with approx. 20 bases and a melting temperature of about 60°C [6] were designed using Primer3-Plus.com [26] (Supplementary Table 2). For the comparison of the mRNA level of different genes, the detected cycle thresholds (Ct) were normalised to β-actin (Actb) expression by calculating $\Delta Ct = (Ct_{Actb} - Ct_{Gene\ of\ interest})$ with a detection limit of 10^{-5}.

2.7. Immunocytochemistry

MDCK-II (on coverslips coated with poly-L-lysine hydrobromide; 25 μg/ml) and bEnd.3 cells (rat-tail collagen coating, Roche; 0.67 mg/ml in 0.2% acetic acid) were fixed in ice-cold acetone (5 min), ethanol (1 min) and PBS (2 min). After blocking (2% bovine serum albumin, Roth, Karlsruhe, Germany, 0.05% Triton X-100 in PBS; 45 min), cells were incubated with primary antibodies at 4 °C overnight. Then, four wash steps (à 5 min, PBS) were followed by 1 h incubation with secondary antibodies, four washings (5 min, PBS), short immersion in dist. H_2O, and embedding in Roti-mount FluorCare DAPI (Roth). Antibodies were from Thermo Fisher Scientific (claudin-5, ZO-1), from Cell Signalling Technologies, Leiden, Netherlands (non-phospho (S45) β-catenin, phospho (T24) FoxO1 (#9464)), from AbD Serotec, Puchheim, Germany (GAPDH), from Biozol, Eching, Germany (ZO-1), and from R&D Systems, Minneapolis, USA (VE-cadherin). For dilutions and host, please refer to Supplementary Table 3. Stably expressing HEK-293 YFP-Cldn or Cldn-YFP were analysed via live cell imaging. For live cell imaging, cell membranes were stained with a few drops of trypan blue solution (0.4%; Gibco). Fluorescence was measured by using a LSM 710 Confocal Microscope System with EC Plan Neofluar 40×/1.3 or Plan apo 63×/1.4 oil-objectives and ZEN Image Browser Software (Zeiss, Jena, Germany). Fluorescence intensities were quantified by ImageJ (NIH, Bethesda, USA), setting defined lines around the plasma membranes [22]. For *trans*-interaction, the fluorescently labelled claudin peaks on the intensity profiles along the line connecting the centres of two neighbouring HEK-293 cells were used to identify claudin-enriched contacts between two claudin expressing cells. The contact enrichment (E_F) was applied to investigate the effect of M01 on the cell-to-cell binding [27].

2.8. Immunoblotting

bEnd.3 cells were washed (PBS), lysed in ice-cold buffer (100 mM NaCl, 20 mM Tris/HCl, 1 mM $MgCl_2$, 0.1% Triton X-100, 5% glycerol,

benzonase 20 U/ml with protease inhibitor (Roche), pH 7.5), homogenized with a 25-G needle and centrifuged (4 °C, 10 min, 12,000 ×*g*). The supernatant was dissolved in sample buffer (0.225 M Tris/HCl, 50% glycerol, 5% Na-dodecyl sulphate, 0.05% bromophenol blue, 0.25 M dithiothreitol, pH 6.8), heated at 95 °C for 5 min (claudins 55 °C, 15 min), and loaded on a polyacrylamide gel. Gels were run at 120 V in running buffer (25 mM Tris/HCl, 192 mM glycine, 0.1% Na-dodecyl sulphate, pH 8.3) for about 90 min. After separation, proteins were transferred on a nitrocellulose membrane (Bio-Rad Laboratories, München, Germany) at 4 °C and 100 V for 1 h and tested for the respective antibodies (Supplementary Table 3) at 4 °C overnight.

2.9. M01 solubilisation

The solubility properties of M01 were determined spectrophotometrically (Spectrophotometer J-720, Jasco, Japan). Absorption spectra of 30 μM M01 in 1% DMSO dissolved in HBSS, M01 in 20% 2-hydroxypropyl-β-cyclodextrin (HPβCD) or HPβCD alone were taken in the wavelength range from 270 nm to 450 nm.

2.10. Brain uptake studies, animal treatment, and glioma model

For investigation of the BBB, adult C57BL/6N mice were kept in standard conditions according to German animal welfare law in Berlin (G0030/13, LaGeSo). 650 μM M01 in PBS with 1% DMSO, 20% (HPβCD, 4.5 μl/g b.w.) were administered into the tail vein resulting in 65 μM blood concentration; the injection was repeated 18 and 21 h later. The fluorescein uptake experiment was performed 3, 6, 12, 24 or 48 h after the final M01 treatment. Na-fluorescein (2%, 376 Da, Sigma-Aldrich) was injected i.v. (4.5 μl/g b.w.) 15 min after M01, while the mice were anesthetized (0.18 mg/g b.w. ketamine; CP-Pharma, Burgdorf, Germany; 0.024 mg/g b.w. xylazine; Ceva Tiergesundheit, Düsseldorf, Germany; i.p.). A volume of 25 ml PBS containing 6250 IU sodium heparin (Ratiopharm, Ulm, Germany) was perfused (1.5 ml/min) through the left ventricle of the heart. To evaluate Na-fluorescein, 100 mg tissue was homogenized in 250 μl PBS followed by precipitation with 250 μl 60% trichloric acid (>2 h, 4 °C) and centrifugation (18,000 ×*g*, 20 min 4 °C). The fluorescence (λ_{ex} 485 nm/λ_{em} 520 nm) of the supernatant was determined using a Tecan plate reader. Brain uptake was calculated as μg fluorescein/mg brain [22] and normalised to brain uptake after control treatment (PBS, 3 h).

In concert, the triple administration of 2.9 μmol/kg M01 (and 5.8 μmol/kg), a 20% and 40% HPβCD solution (600 and 1200 μmol/kg), and 1% and 2% DMSO (1.2 and 2.4 mmol/kg) did not exert any toxic effects. The mice grew normally (Supplementary Fig. 1) and without alterations in their appearance and behaviour (for example: grooming, breathing rate, signs of pain, activity, ingestion) even after weekly repetition over four weeks. For the glioma model, 20,000 U-87 MG cells (glioblastoma/astrocytoma grade IV, 44 y old male Caucasian [28]) were intracranially inoculated in immunodeficient NMRI-Foxn1 $nu^{-/-}$ mice. Five days after injection of the cells, the mice received the triple administration procedure with M01 in HPβCD or PBS. Three hours after the third M01 injection, the mice were treated with 28 μmol/kg paclitaxel or PBS as control (8 mice per group). The mice were weighed daily. The treatment scheme was repeated once a week for 4 weeks in total. Afterwards, the mice were euthanized, and the brains harvested. For quantitative evaluation of U87-MG glioma growth, the entire tumour containing area was cryosectioned. Consecutive cryosections were fixed with methanol (10 min, −20 °C), washed with dist. H_2O, incubated with cresyl violet (0.1%, 10 min), and shortly treated with dist. H_2O followed by 0.1% HCl. After dehydration and embedding in Roti Histo Kit (Roth), for each animal the brain slice with the largest tumour area was used for quantification (Sigma Scan Pro, Systat Software, San Jose, USA) [29]. For the determination of the compound and metabolite concentration in serum, blood samples were taken from the tail vein of mice at time points 0.083, 0.25, 0.5, 1, 3, 7 h after tail vein injection of 1.5 mg/kg M01, M01B or HPβCD ($n = 3$). For the quantification of excreted compounds, mice were transferred in metabolic cages for 24 h after injection. Afterwards, concentrations in urine and faeces (n = 3) were determined by LC-MS (Pharmacelsus GmbH, Saarbrücken, Germany).

2.11. Molecular modelling, docking, and statistics

The interaction surface between M01 and murine claudin-5 was modelled using SwissDock [30] based on the structure prediction of the claudin which was performed using Iterative Threading ASSEmbly Refinement (I-TASSER) [31]. The modelling also considered the experimental data. If not stated otherwise, data were analysed using the Kruskal-Wallis test (one-way ANOVA) followed by Dunn's multiple comparison post-test. Statistics and graphs were generated using GraphPad Prism5.

3. Results

M01 (Fig. 1A) was identified in a screening approach searching for molecules reducing claudin-5 (Cldn5) expression and cell-cell contact enrichment. HEK-293 cells are free of endogenous claudin expression [32]. In YFP-Cldn5 or YFP expressing HEK-293 cells, incubation with 20 μM M01 overnight reduced the fluorescence intensity of YFP-Cldn5 significantly but not the intensity of YFP (Fig. 1B).

Next, we determined the effect of M01 on the homophilic claudin-5/claudin-5 *trans*-association as detected by contact enrichment of claudin-5 between HEK-293 cells transfected with YFP-tagged claudin-5. Fig. 2A demonstrates that the fluorescence intensity of claudin-5 in cell contacts decreased with increased M01 concentrations. The effect was reversible as the fluorescence at the contacts recovered within 48 h (image Fig. 2A, bottom right). A reduction in junctional enrichment occurred within the first 3 h after incubation and became evident after 17 h if more than 10 μM M01 were applied (Fig. 2A, B). After 48 h with M01 treatment, the junctional enrichment of claudin-5 was not different from the claudin-5 enrichment of the control treatment. However, merely a slight effect on TJ-like strands was observed after 17 h in freeze fracture electron microscopy (Supplementary Fig. 4). The effect of M01 was mostly directed towards claudin-5 as demonstrated for HEK-293 cells transfected with TJ forming BBB claudins-1 (compared to DMSO control, E_F: 99.1% ± 9.05%), −3 (E_F: 95.2% ± 21.8%) and − 4 (E_F: 102.0% ±10.4%; Fig. 2C). Using microscale thermophoresis, the preferential interaction of M01 with full-length claudin-5 (K_d: 237.7 ± 31.7 nM) in cell extracts was quantified. In addition, a lower affinity to claudin-3 (K_d: 935.1 ± 199.6 nM) was found while dissociation constants for other claudins were more than one order of magnitude lower than for claudin-5 (Fig. 2D). The claudin-5 specificity and the M01 effect on barrier permeability was further proved by permeability assays with MDCK-II cells. These were stably transfected with a flag-Cldn5 construct or with the empty vector alone. MDCK-II cells endogenously express claudins 1, 2, 3, 4, and 7 [15,33] and form a tissue barrier-like monolayer with typical transepithelial electrical resistance (TER) of ~100 Ω x cm [2,15]. M01 increased the permeability of the small dye Lucifer yellow (LY, 457 Da, Fig. 2E) in a concentration-dependent manner (MDCK-II-flag-Cldn5 control P_{app}: $0.875 \pm 0.158 \cdot 10^{-5}$ cm/s; MDCK-II wildtype control P_{app}: $0.693 \pm 0.188 \cdot 10^{-5}$ cm/s). It also decreased the TER (Fig. 2F) of flag-Cldn5 transfected MDCK-II, but not of cells expressing endogenous claudins alone. The treatment of MDCK-II-flag-Cldn5 cells with 50 μM M01 led to intracellular accumulation of claudin-5, whereas the solvent DMSO had no effect on the subcellular localisation (Fig. 2G).

As claudin-5 deficient mice showed a BBB phenotype only [7], the main target of M01 should be the brain microvascular endothelium. Thus, the effect of M01 was confirmed in bEnd.3 cells, a cell culture model of the BBB. Among claudins, this cell line mainly expresses claudin-5 and, to a lower degree, claudin-12 (two orders of magnitude less mRNA), claudin-1 and claudin-3 (four orders less, see also Fig. 4A)

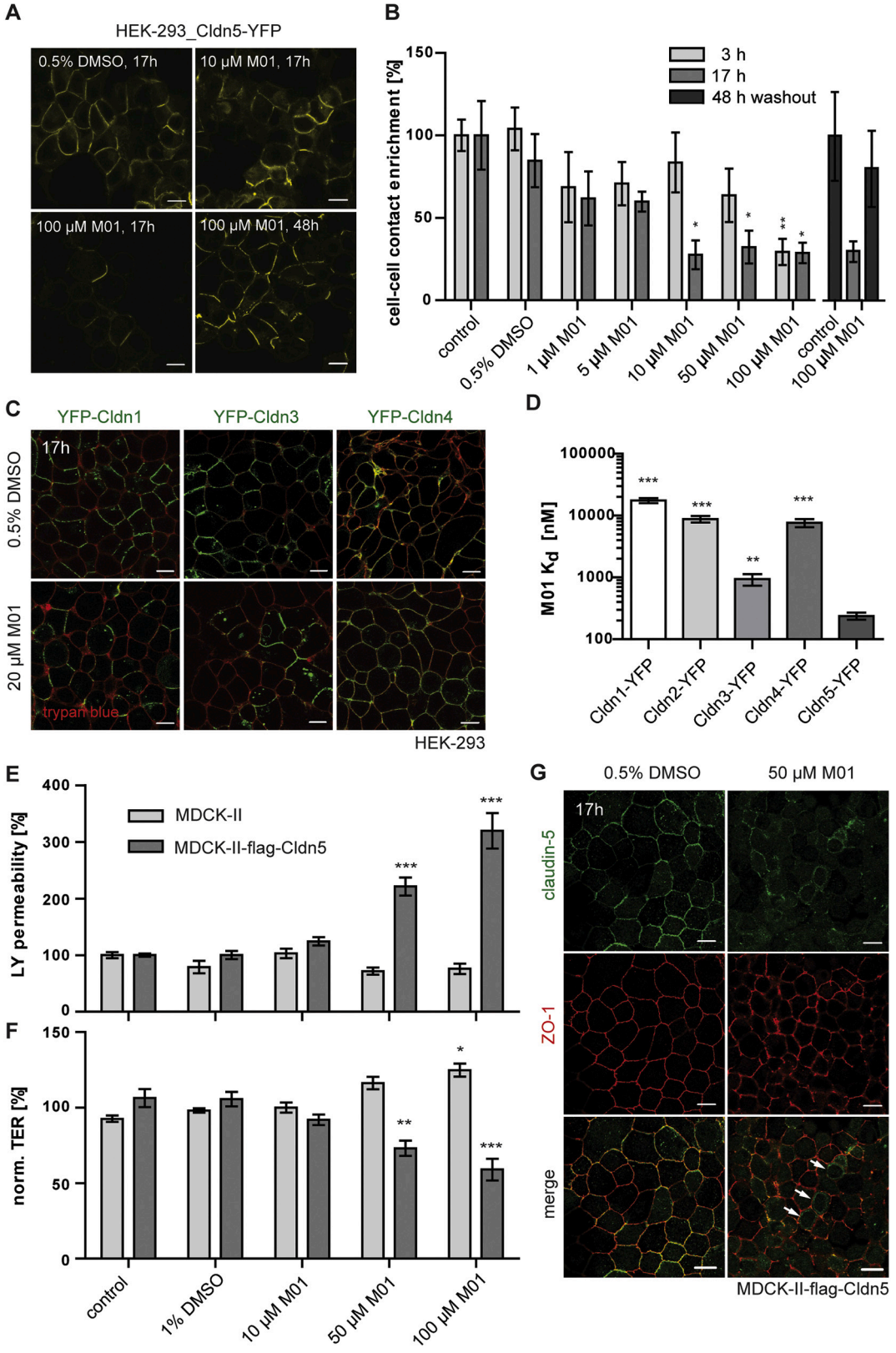

(caption on next page)

Fig. 2. The effect of M01 on claudin-5 is highly specific, time and concentration dependent followed by internalization. A) As a measure for the M01 effect on claudin-5 (Cldn5), *trans*-interactions were calculated as fluorescence intensity enrichment in cell-cell contacts between HEK-293 cells transfected with Cldn5-YFP compared to the control. After treatment with M01 the Cldn5-YFP fluorescence recovered within 48 h. B) Column diagram of the calculated Cldn5-YFP enrichment at cell-cell contacts in HEK-293 cells. The effect was time- and concentration dependent. The contact enrichment level of M01 treated HEK-293 cells returned to control values after 48 h ($n \geq 6$ images). C) No effect of 20 μM M01 was observed on other BBB claudins in HEK-293 cells. Cells were transfected with YFP-Cldn1, YFP-Cldn3 and YFP-Cldn4 (green) and the cell membranes stained with trypan blue (red). D) Dissociation constants (K_d) of M01 and Cldns 1 to 5 determined by microscale thermophoresis (n ≥ 6 experiments). Data are shown as mean ± SEM. Two-tailed Mann-Whitney test compared to Cldn5, **, $p < 0.005$; ***, $p \leq 0.0003$. E) Lucifer yellow (LY, 444 Da) permeability, and F) transcellular electrical resistance (TER) of MDCK-II (t_0: ~80 Ω·cm^2) and MDCK-II-flag-Cldn5 (t_0: ~100 Ω·cm^2) monolayer treated overnight with different concentrations of M01 (n ≥ 6 filter). LY permeability was normalised to the respective control values (untreated). The TER values after treatment were normalised with the values before treatment. G) Immunofluorescence staining of MDCK-II and MDCK-II-flag-Cldn5 cells after overnight incubation with M01. Claudin-5 (green) was visualised with a rabbit anti-Cldn5 antibody. For the junctional marker ZO-1 (red) mouse anti-ZO-1 was used. The arrows point at examples for internalised Cldn5 after M01 treatment. If not stated otherwise, Kruskal-Wallis-test followed by Dunn's multiple comparison-test was used. Mean ± SEM; *, $p \leq 0.05$; **, $p \leq 0.01$; ***, $p \leq 0.001$; significance related to DMSO control. Scale bar = 10 μm. (For interpretation of the references to colour in this figure legend, the reader is referred to the web version of this article.)

[6]. M01 interaction with claudin-5 led to a reduction of claudin-5 in bEnd.3 cells in both plasma membrane and cytosol (50% reduction in membrane, 43% in the cytosol) within 16 h after the addition of 50 μM M01 (Fig. 3A, B upper diagram). A slight but significant decrease of claudin-5 membranous and intracellular fluorescence intensity was observed for M01A (9% and 12%, respectively) and M01B (15% and 32%, respectively). M01A and M01B represent the two molecular parts of M01, which have been studied to identify the active part of M01. For ZO-1, the junctional scaffolding protein, only a slight difference in their fluorescence was observed between treatments (Fig. 3A, B lower diagram). However, M01 (Fig. 3C), but neither M01A nor B (Fig. 3D), affected the barrier properties of bEND.3 cells. The TER decreased immediately after administration of ≥7.5 μM M01. The maximum effect ion permeability was dependent on the concentration: 7.5 μM M01 caused 18% reduction after 10 h, and 50 μM M01 caused 39% reduction after 23 h (Fig. 3C). Afterwards, the TER recovered slowly.

The permeabilising effect of M01 in endothelial cells was accompanied by claudin-5 decline after overnight treatment. M01 (50 μM) decreased the protein amount by 73% (Fig. 3E). Again, the protein amount of claudin-5 was not significantly reduced after 50 μM M01A treatment, but decreased after applying 50 μM M01B (by 41%). Incubation of bEND.3 cells for 48 or 72 h with 20 μM M01 did not further decrease the claudin-5 protein amount, but washout of M01 after 17 h and cultivation for another 31 or 55 h in complete medium led to recovery of claudin-5 expression (Fig. 3F). The junctional localization of claudin-5 also recovered after M01 washout (Supplementary Fig. 2). The compounds M01, M01A and M01B were nontoxic for brain endothelial cells and for epithelial cells, at least up to 50 μM (Supplementary Fig. 3).

We previously described the decrease of claudin-5 mRNA level of bEND.3 cells after claudin-5-peptide treatment [22]. Therefore, we examined the transcription of several TJ proteins after treatment of bEND.3 cells with 15 or 50 μM M01. The mRNA level of claudin-5 decreased by about 81% after incubation with 50 μM M01 for 16 h. Transcription of other claudins and occludin was not significantly affected, but the level of ZO-1 mRNA declined by about 62% (Fig. 4A). The non-phosphorylated, active forms of the transcription factors β-catenin and FoxO1 (Fig.4B) establish a known claudin-5 repressor complex in endothelial cells. Under normal conditions, β-catenin is sequestered at adherens junctions with VE-cadherin. If the junctional complex is disturbed, the degradation of intracellular active β-catenin is inhibited, or higher β-catenin expression occurs, leading to intracellular accumulation of active β-catenin. FoxO1 and β-catenin shuttle to the nucleus, interact with each other and inhibit claudin-5 transcription (Fig. 4B) [34,37]. Consistent with this model, down-regulation of claudin-5 was paralleled by an increased amount of non-phosphorylated (S45) β-catenin in M01-treated endothelial cells as demonstrated by immunofluorescence staining (Fig. 4C). Quantification of the fluorescence intensity revealed higher signals in both cell membrane and cytosol (Fig. 4D). The cellular increase was confirmed by immunoblotting, showing an elevated amount of non-phosphorylated (S45) β-catenin after overnight treatment with M01 (Fig. 4E). In parallel to β-catenin, the phosphorylation level of FoxO1 at Thr24 was slightly reduced after M01 treatment (Fig. 4F). Other junctional proteins of the model were affected as well: VE-cadherin and the total protein amount of β-catenin slightly increased after 17 and 48 h M01 treatment and recovered after washout (Fig. 4G). As observed for the bEnd.3 immunofluorescence stainings (Fig. 3A), ZO-1 was not reduced after 17 h M01 incubation (Fig. 4G). However, the ZO-1 level decreased after 48 h of treatment with M01 and showed strongest reduction after washout of M01 (Fig. 4G).

Next, we examined the efficacy of M01 in vivo. Because of the hydrophobic character of M01, the solubility in aqueous solution had to be increased for in vivo application. M01 is soluble in pure DMSO until 65 mM. To reach at least the in vitro efficacious concentration of 50 μM, we had to inject 100 μl of 650 μM M01 dissolved in PBS i.v. (~1.3 ml blood volume per mouse) without increasing the final DMSO concentration above 1% or exceeding the maximum injectable volume (≤10% of blood volume). Therefore, HPβCD was utilized as an in vivo well tolerated solubility enhancer [38]. In a 20% HPβCD solution, 650 μM M01 dissolved finally (Supplementary Fig. 5; final concentration DMSO: 1%). The tolerability of M01, DMSO and/or HPβCD in mice was tested before further in vivo experiments. Mice received weekly injections for 4 weeks without showing any symptoms (e.g., weight loss, Supplementary Fig. 1). Pharmacokinetic experiments determined a half-life ($t_{1/2z}$) for M01 in blood plasma of 18 min and for HPβCD of 66 min in mice (Supplementary Fig. 6). Besides M01 and HPβCD, nalidixic acid (M01A) was found as a metabolite in blood serum of mice after M01 injection with a maximal concentration (C_{max}) of 2.2278 μM (517.3 ng/ml) after 6 min and a $t_{1/2z}$ of 48 min. M01B was not detected.

Based on the pharmacokinetic and toxicity experiments, the efficacy of M01 to permeabilise the BBB was investigated with an in vivo BBB sodium fluorescein permeability assay (Fig. 5A, top). Single injections of M01 in HPβCD did not increase the fluorescein amount in the brain tissue. Thus, we tested a variety of different injection patterns. Fig. 5A shows the data for the final triple i.v. injection procedure (18 h + 3 h + 3 h) of 2.9 μmol/kg M01 in 600 μmol/kg HPβCD into C57/BL6N mice. The maximum brain uptake of the small molecule Na-fluorescein (367 Da) was found at a level of 1.5 ± 0.2 nmol/g tissue, 3 h after final injection. The uptake was detectable up to 48 h (Fig. 5A, diagram on the left). However, after ~10 h no difference compared to the effect of HPβCD alone was observed. The mild permeability increase due to HPβCD alone was constantly detectable between 3 and 24 h. Liver tissue served as negative control and did not show changes in the uptake of fluorescein after M01 administration (Fig. 5A, diagram on the right).

Mice bearing orthotopic glioblastoma xenografts (human U-87 MG cells) were investigated to provide evidence for improved drug delivery by M01 to the brain (Fig. 5B). Three hours after the final weekly M01 administration, 28 μmol/kg (24 mg/kg) of the cytostatic drug paclitaxel (854 Da) were applied (40 μl/g b.w., i.v.), which was repeated weekly for four weeks. Paclitaxel had no effect on tumour growth when administered alone (Fig. 5B, upper brain section). However, when given in combination with M01, paclitaxel administration resulted in a

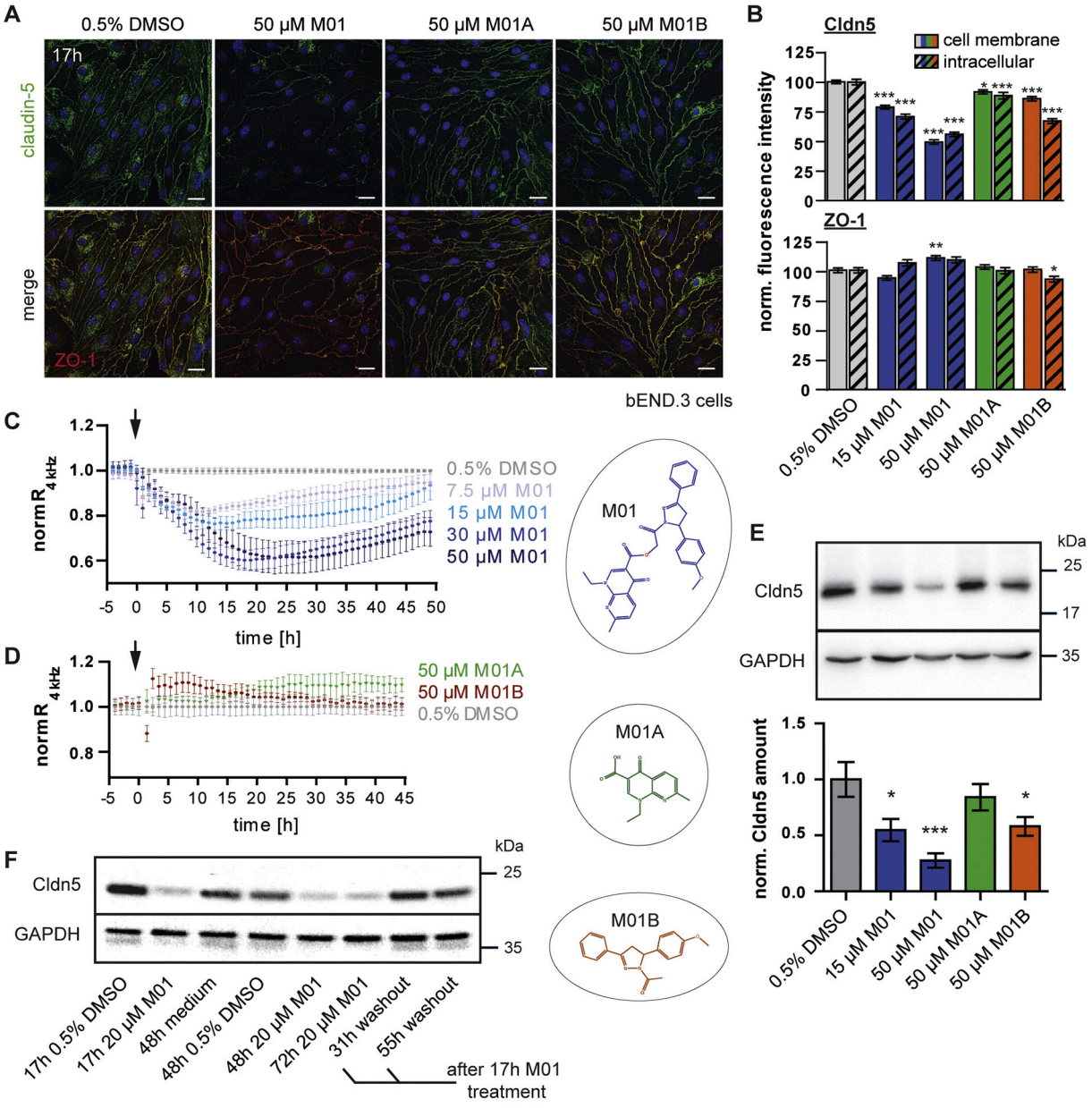

Fig. 3. M01A and M01B are much less effective in decreasing endothelial tight junction functions than M01. A) Monolayer formed by murine brain endothelial (bEND.3) cells, a BBB tissue culture model, expressing endogenously claudin-5 (green) were treated with 50 µM M01, M01A (nalidixic acid) or B (3-phenyl-5-methoxyphenyl-1H-pyrazole) for 16 h. For immunofluorescence staining the antibodies mouse anti-Cldn5, rabbit anti-ZO-1, and DAPI for the nuclei were used. Scale bar = 20 µm. B) Quantification of the fluorescence intensity of claudin-5 (upper diagram) and ZO-1 (lower diagram) at the cell membrane and intracellular after treatment with M01, M01A or M01B compared to DMSO treated bEND.3 cells. Mean ± SEM, $n > 200$ cells. Kruskal-Wallis-test followed by Dunn's multiple comparison-test. Mean ± SEM; *, $p \leq 0.05$; **, $p \leq 0.01$; ***, $p \leq 0.001$. C) and D) impedance was determined by electric cell-substrate impedance sensing (ECIS) at 4000 Hz. Values were shown as normalised to impedance values before treatment with different concentrations of M01 (C) or 50 µM M01A and M01B (D). The arrow indicates the beginning of the treatment of the bEnd.3 monolayer. Mean ± SEM, $n \geq 4$ experiments. E) M01 and slightly M01B reduced the protein expression of claudin-5, immunoblot quantification corrected by GAPDH values. Mean ± SEM, $n = 7$ immunoblots. One-way-ANOVA and Dunnett's multiple comparison test; *, $p \leq 0.05$ and ***, $p \leq 0.001$ vs. DMSO. F) Immunoblot of bEND.3 cells treated for 17, 48 and 72 h with M01 and recovery after 17 h M01, M01 washout and culture medium for 31 h and 55 h ($n = 3$ blots). (For interpretation of the references to colour in this figure legend, the reader is referred to the web version of this article.)

significant reduction of the tumour size. The mean tumour size was only 22% of the size of those mice, which received paclitaxel alone (Fig. 5B, lower section, diagram).

To exclude the possibility of cytotoxicity by M01 or HPβCD for U-87 MG cells, which might lead to decreased tumour growth, an in vitro cytotoxicity assay was performed. Even in combination, the cells were not affected by 0.5% DMSO, 1.5% HPβCD, and 50 µM M01 (in 0.5% DMSO). After 10 µM paclitaxel treatment the viability was decreased to 55%, which was further reduced to 35% by combined treatment with HPβCD and M01 in DMSO (Fig. 5C).

4. Discussion

In general, the physio-chemical properties of M01 (table in Fig. 1A) satisfy the demands on oral bioavailability [9,23] and parenteral administration of a pharmaceutical product. Its molecular weight is in the range of 500 Da and the cLogP is 2.8. Such a cLogP is indicative of a suitable lipid- and water solubility and allows fair binding at

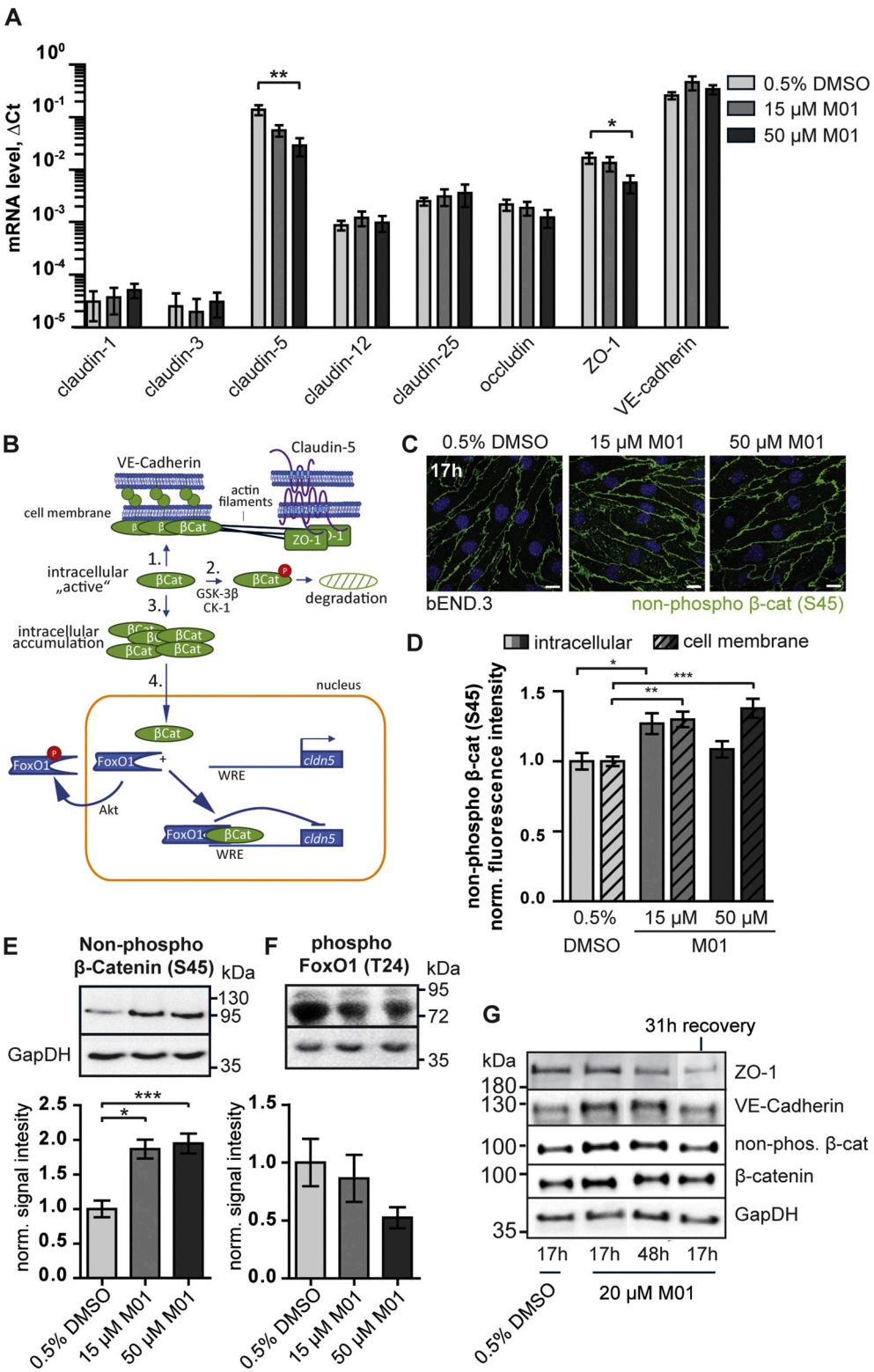

Fig. 4. M01 is inhibiting claudin-5 expression in brain endothelial cells, at protein and mRNA level. A) mRNA expression of junctional proteins in bEnd.3 cells detected by qRT-PCR (ΔC_T, cycle threshold normalised to β-actin), 16 h incubation, M01 in 0.5% DMSO. Mean ± SEM, $n = 6$ experiments. ZO-1, *Zonula occludens* protein 1; VE-cadherin, vascular endothelial cadherin. B) Sketch of claudin-5 expression inhibition by the active, non-phosphorylated form of β-catenin and forkhead box protein O1 (FoxO1). 1. Under normal, barrier-forming conditions, β-catenin accumulates at the cell membrane bound to the adherens junctional complex. 2. Intercellular β-catenin is phosphorylated and subsequently degraded. 3. Inhibition of the β-catenin destruction complex leads to accumulation of intracellular β-catenin, which shuttles into the nucleus. 4. Together with FoxO1, β-catenin functions as a claudin-5 transcription inhibitor binding to the Wnt response element (WRE) in the promotor region [34–36]. C) Immunofluorescence staining of bEnd.3 cells 16 h after incubation with 15 and 50 μM M01. S45 non-phosphorylated "active" β-catenin (rabbit, green) is known to be able to shuttle into the nuclei (blue, DAPI) and acts as a repressor of Cldn5 transcription [34]. M01 intensified the membrane and intracellular localisation of S45 non-phosphorylated β-catenin. Scale bar, 10 μm. D) Quantification of cellular distribution, mean ± SEM, $n \geq 21$ images. E) and F) immunoblot and quantification of E) non-phospho (S45) β-catenin (β-cat, 92 kDa) and F) phospho (T24) FoxO1 (72–85 and 95 kDa) normalised to GAPDH (36 kDa). Mean ± SEM, n = 6 blots. One-way-ANOVA and Dunnett's multiple comparison test. *, $p \leq 0.001$. G) Immunoblots of ZO-1, VE-cadherin, non-phospho (S45) β-catenin and β-catenin after M01 treatment and recovery for 31 h in culture medium, $n \geq 3$ immunoblots. If not stated otherwise Kruskal-Wallis-test followed by Dunn's multiple comparison-test was used. *, $p \leq 0.05$; **, $p \leq 0.01$; ***, $p \leq 0.001$. (For interpretation of the references to colour in this figure legend, the reader is referred to the web version of this article.)

intramembranous and soluble parts of transmembrane proteins, such as claudin-5, which was targeted in this study. The number of HB-acceptors and -donators as well as the number of rotating bonds is in the required range (≤10, ≤5 and ≤ 10, respectively [9,23]), thus providing flexibility necessary to adapt to the highly dynamic function of claudin-5 within the TJs [24]. This coincides with our docking studies. The resulting interaction model shows a preferred association of M01 to the extracellular domain and an adhering outward-directed transmembrane patch of the claudin (Fig. 6).

Compounds envisioned to improve drug delivery through pharmacological barriers - termed drug enhancers - are required to exhibit a high affinity to a tissue-specific target and a transient and moderate barrier permeabilisation. M01 meets these requirements at the BBB. It associates with claudin-5, whose knockout causes a specific BBB phenotype [7], and it acts in a low micromolar range. Dissociation constants found for other barrier-forming claudins are at least 3.93 times

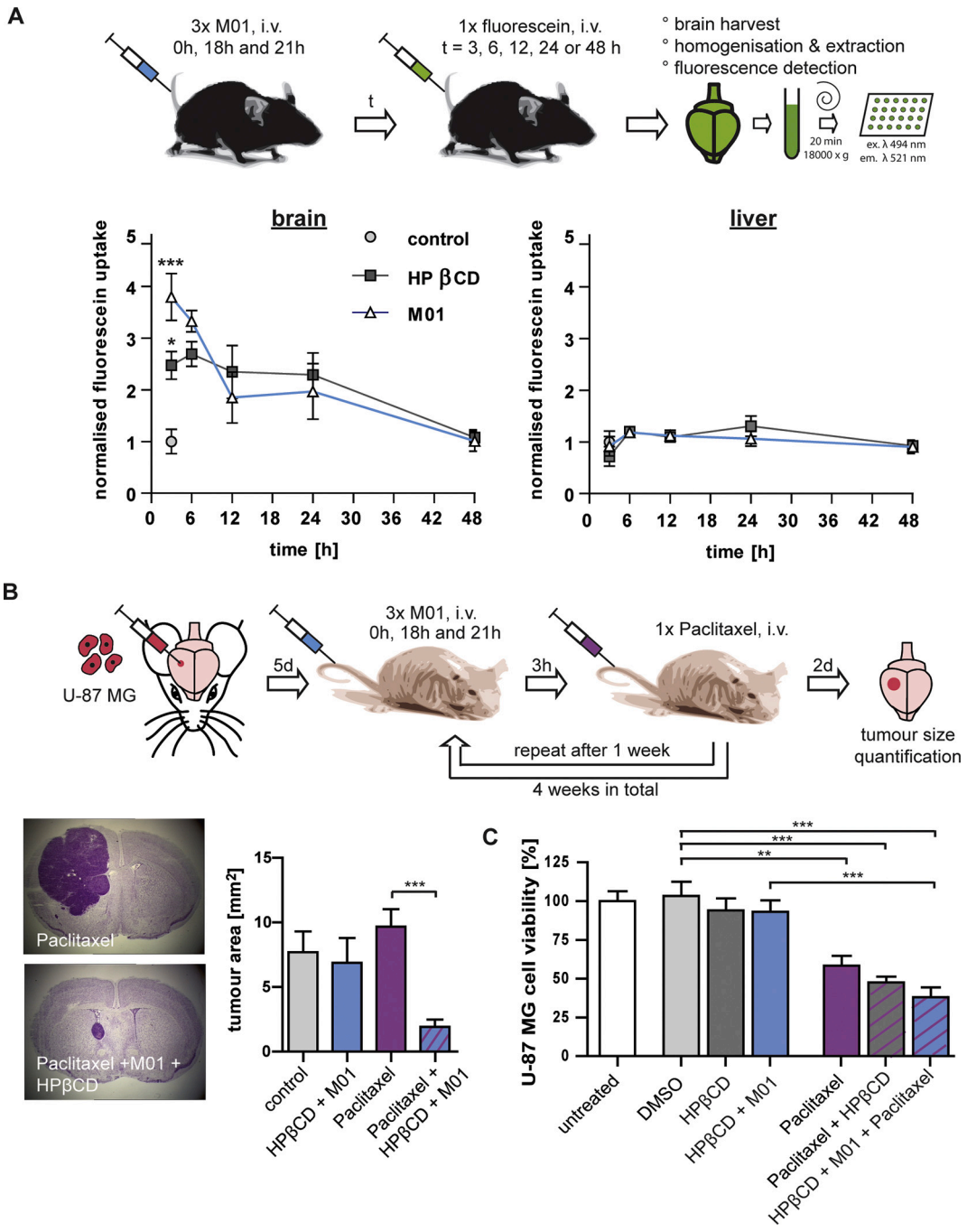

Fig. 5. M01 transiently permeabilises the blood-brain barrier for small molecules in vivo and enables paclitaxel to inhibit brain tumour growth. (A) Permeabilisation of the murine blood-brain barrier by M01 as determined by cerebral fluorescein uptake. 2.9 μmol/kg M01 in 600 μmol/kg HPβCD (2-hydroxypropyl-β-cyclodextrin), 600 μmol/kg HPβCD or $PBS^{+/+}$ (phosphate buffered solution with Ca^{2+}/Mg^{2+}) were administered three times into the tail vein at 0, 18 and 21 h. 242 μmol/kg Na-fluorescein (367 Da) was injected into the tail vein at different time points after the last M01 treatment. Mean ± SEM, $n = 3$–15 mice. (B) For the experimental treatment of an orthotopic glioma model, human U-87 MG cells were administered intrathecally into immunodeficient NMRI-Foxn1 $nu^{-/-}$ mice. After five days, mice were treated once a week (i.v.) for four weeks with 28 μmol/kg paclitaxel alone or paclitaxel together with M01 in HPβCD (administration pattern: 0/18/21 h M01 and 3 h later paclitaxel). Left: cresyl violet staining of 10 μm cryogenic brain sections. Tumour tissue stained in dark violet. Mean ± SEM, $n = 6$–8 mice. C) Viability (MTT) assay to prove sensitivity of U-87 MG cells to paclitaxel and M01. Cell Monolayer were treated with 0.5% DMSO, 1.5% HPβCD, 50 μM M01, 10 μM paclitaxel or in combinations. Values were calculated in comparison to untreated cells in percent. A, B and C: Kruskal-Wallis-test with Dunn's multiple comparison test; *, $p \leq 0.05$; **, $p \leq 0.01$; ***, $p \leq 0.001$. (For interpretation of the references to colour in this figure legend, the reader is referred to the web version of this article.)

lower, and their individual expression at the BBB is less than 1% of claudin-5 [6]. In addition, if claudin-5 is additionally expressed, M01 specifically enhances the permeability of a small molecular weight marker (LY) through MDCK-II, a TJ- and barrier-forming cell layer [21]. In mouse experiments, the permeability of fluorescein through the BBB is four times enhanced, peaks after three hours and returns to the level of HPβCD permeability within 6 to 12 h. It should be mentioned that the maximum uptake of 1.5 ± 0.2 nmol fluorescein per g brain tissue depends on the detection method we used, application of other methods might yield different results. A smaller, longer lasting permeability increase might be caused by HPβCD. Cyclodextrins can remove cholesterol from cell membranes and thus, the permeability of barrier forming cell

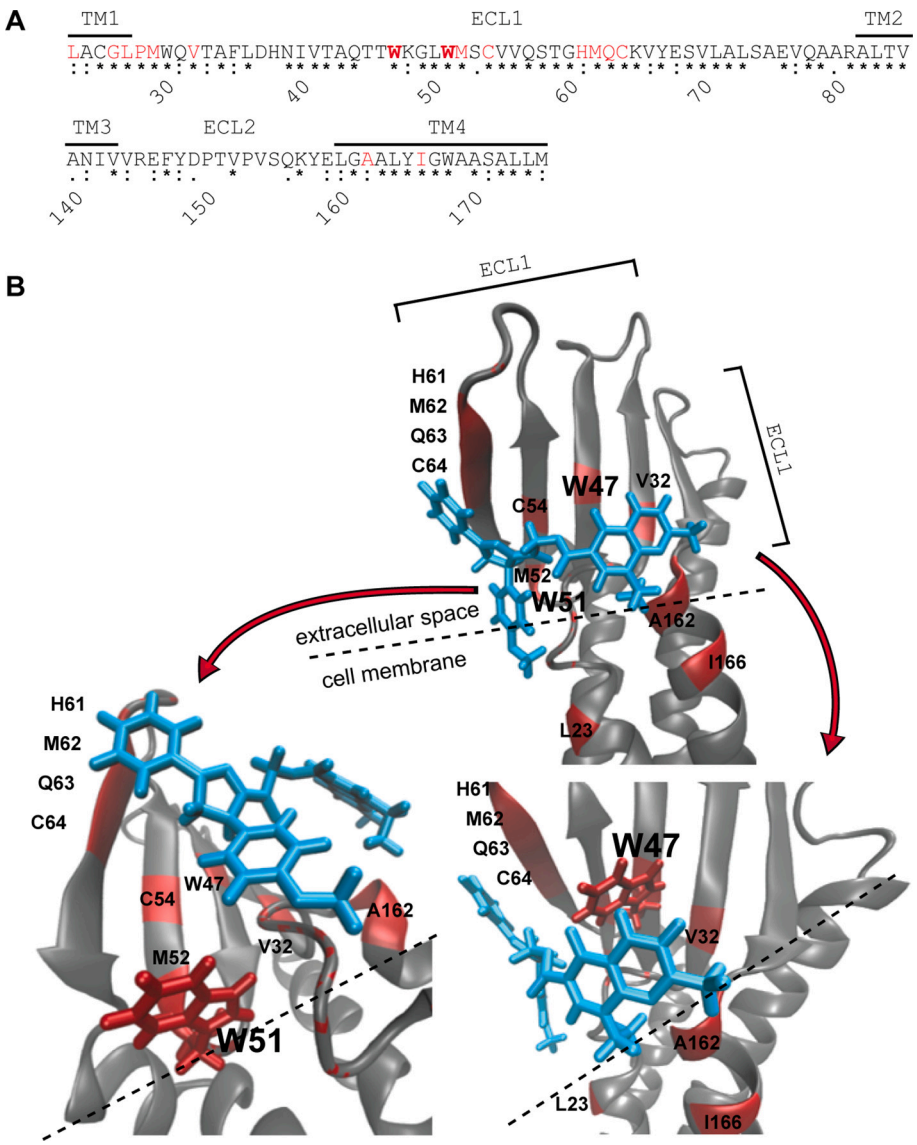

Fig. 6. 3D-interaction model between M01 (blue) and extracellular loop (ECL) domain with adjoining transmembrane domains (TMs) of murine claudin-5. The proposed binding area predominantly consists of a β-sheet including five β-strands (four from ECL1, one from ECL2) flanked by an α-helix (from ECL2); red amino acids: distance to M01 ≤ 4.5 Å. A) Amino acid sequence of claudin-5 ECLs and neighbourhood: (*), in Mammalia conserved claudin-5 residues; (:), strongly similar; (.), weakly similar; red, residues in binding distance (≤4.5 Å). B) Interaction model between M01 and claudin-5 (ribbon model) as energetically favourable conformation (SwissDock, [30]), with particular consideration of aromatic interaction sites (W47 right inset, W51 left inset). Structural prediction of claudin-5 [31] adapted from crystal structure of claudin-15 [13]. Dashed lines, predicted extracellular membrane surfaces. (For interpretation of the references to colour in this figure legend, the reader is referred to the web version of this article.)

monolayer is increasing [39,40]. Taken together, these results suggest that M01, perhaps in synergy with HPβCD, permeabilises the BBB preferentially via claudin-5, moderately and for a short time. The strength and duration of the effect has the potential to facilitate drug permeation through the BBB.

The short-term action of M01 is due to fast retention, metabolisation and degradation (Supplementary Fig. 6). Only traces of M01 and its nalidixic acid part, but not the 3-phenyl-5-methoxyphenyl-1H-pyrazole part of M01 are detectable in urine and faeces. Tolerance studies with weekly administration over four weeks did not affect behaviour, growth, or appearance of the treated mice. M01 and possible metabolites seemed to be well tolerated in mice. These results also support the assumption, that a low-grade and partial permeabilisation of the BBB is non-hazardous. Similar tolerability is observed after short-term permeabilisation of the BBB by a claudin-5 peptidomimetic [22].

The high and mostly specific M01 affinity to claudin-5 accounts for its mode of action. Initially, the M01 binding at the extracellular domain partially suspends the *trans*-interaction. This disturbs the TJ structure, which, in turn, temporarily reduces the intercellular tightness for small-sized drugs, such as cytostatics. A similar effect is assumed after administration of mannitol, a drug enhancer applied in lymphoma therapy [41]. This drastic and unspecific procedure breaches the BBB by osmotic shrinkage of the endothelium, thus completely opening TJs between cells [42]. It bears a high risk of side effects by uptake of larger molecules and cells into the brain. Moreover, a low efficacy has been reported for a considerable number of patients [43]. If mannitol fails to render the BBB permeable, chemotherapeutic drugs do not reach the tumour behind the intact barrier, and the disease will progress [41]. Besides mannitol, other unspecific techniques with harmful side actions have been developed for TJ modulation at the BBB. Highly intensive and focused ultrasound increases delivery of chemotherapeutic drugs in a glioblastoma model [44] after complete BBB breakdown [45]. Vascular endothelial growth factor administration results, among other effects, in downregulation of claudin-5 and impairment of TJs, as shown for delivery of doxorubicin-loaded nanoparticles [46]. But it also opens the BBB for large molecules and causes unspecific alterations in peripheral organs [47]. Nontoxic targeting of claudin-5 has been suggested via siRNA [48], shRNA [49] or monoclonal antibodies [50]. Compared to the acute action of M01, these approaches show a more persistent permeabilisation of the BBB.

Delayed in time, M01 permeabilises the BBB by reduction of the claudin-5 protein level at the TJs. In this regard, we assume claudin-5 internalization and degradation after incubation with M01. The same effect was observed for a claudin-5 peptidomimetic [22]. This peptide is co-internalised with the cell surface localised claudin-5 leading to reduced claudin-5 protein amount. Surprisingly, the peptide and M01

also affect the claudin-5-transcription (Fig. 4A). The transcription factors β-catenin and FoxO1 are known to regulate claudin-5 in endothelial cells if β-catenin is not sequestered at adherens junctions and its phosphorylation and degradation is inhibited (Fig. 4B) [34,37,50]. In our experiments, VE-cadherin and β-catenin remained at the cell membrane during M01 treatment and their protein amounts increased (Fig. 4A, G). However, we also found increased amounts of non-phospho (S45) β-catenin and a slightly (but not significantly) reduced level of T24-phospho FoxO1 [35,36]. Phosphorylation of FoxO1 by the kinase Akt at T24 leads to nuclear export of FoxO1 [51,52]. Our results support the assumption of M01-induced inhibition of claudin-5 transcription by non-phospho FoxO1 and β-catenin. The reason for increased amounts of active β-catenin and FoxO1 needs further investigations.

For the purpose of a potential modulation of the drug enhancer effect, it is particularly interesting to identify a certain M01 moiety, responsible for BBB permeabilisation and loss of claudin-5. The results indicate that the entire structure is essential for maximum activity. Both the 3-phenyl-5-methoxyphenyl-1H-pyrazole and nalidixic part alone are much less effective. Both parts contain at least one aromatic ring, which is assumed to support interaction between claudin-5 and M01. However, the part with the 3-phenyl-5-methoxyphenyl-1H-pyrazole, which has a larger surface area and higher flexibility, shows more interaction sites towards claudin-5 in the docking model of M01 in comparison to the nalidixic acid part (Fig. 6).

M01 permeabilises the BBB transiently and moderately for small molecules. The drug enhancement activity is verified by application of the cytostatic drug paclitaxel (molecular weight, 854 Da). As reported earlier [53], paclitaxel does not exhibit cytostatic activity for brain tumours. However, it significantly reduces the glioblastoma growth after M01 pre-treatment in an orthotopic xenograft model. Nevertheless, some questions remain, e.g., if the increase of vascular permeability for cytostatic drugs in the non-tumour brain regions induces toxicity on cells of the central nervous system as reported for paclitaxel on astrocytes [54]. Thus, further investigations are necessary to prove the applicability of M01 in brain tumour therapy.

In conclusion, M01 is identified as the first small molecule specifically modulating claudin-5 and permeabilising the BBB for drug-like molecules. The use of M01 for drug delivery through the BBB demonstrates that a targeted approach has a strong potential to improve the chemotherapeutic effectiveness for primary brain tumours and cerebral metastases. Moreover, this concept is not restricted to treatment of neoplasms and should be tested for the pharmacotherapy of other cerebral diseases, such as Alzheimer's disease, epilepsy, or stroke.

Author statement

Olga Breitkreuz-Korff: majority of the Methodology, Investigations with contributions from **Christian Tscheik** (HTS, MST), **Giovanna Del Vecchio** (initial cell experiments, HTS), **Sophie Dithmer** (ECIS) **Hartwig Wolburg:** freeze-fracture EM **Andrea Orthmann and Wolfgang Walther:** mouse tumour model investigations; **Reiner F. Haseloff and Leif Schröder:** writing - review and editing **Ingolf E. Blasig:** Funding acquisition, supervision **Lars Winkler**: Conceptualization, writing - original draft.

Acknowledgments

The investigations were supported by BMBF validation of innovative potential (VIP) program 03 V0647 (EASYPERM). Part of this work was supported by the Dieter Morszeck Stiftung. O.B.K. was responsible for the majority of the work, with contributions from C.T., G.D.V. and S.D. Further contributors were H.W. (freeze-fracture EM); A.O. and W.W. (tumour model experiments); R.F.H. and L.S. (writing the manuscript); I. E.B. and L.W. (design of study and concept of manuscript).

Appendix A. Supplementary data

Supplementary data to this article can be found online at https://doi.org/10.1016/j.jconrel.2021.08.014.

References

[1] D. Gunzel, A.S.L. Yu, Claudins and the modulation of tight junction permeability, Physiol. Rev. 93 (2013) 525–569. Review, https://doi.org/10.1152/physrev.00019.2012.
[2] I.E. Blasig, C. Bellmann, J. Cording, et al., Occludin protein family: oxidative stress and reducing conditions, Antioxid. Redox Signal. 15 (2011) 1195–1219. Review, https://doi.org/10.1089/ars.2010.3542.
[3] G. Krause, L. Winkler, S.L. Mueller, et al., Structure and function of claudins, Biochim. Biophys. Acta-Biomemb. 2008 (1778) 631–645.
[4] G.J. Maher, E.N. Hilton, J.E. Urquhart, et al., The cataract-associated protein TMEM114, and TMEM235, are glycosylated transmembrane proteins that are distinct from claudin family members, FEBS Lett. 585 (2011) 2187–2192, https://doi.org/10.1016/j.febslet.2011.05.060.
[5] R.F. Haseloff, S. Dithmer, L. Winkler, et al., Transmembrane proteins of the tight junctions at the blood-brain barrier: structural and functional aspects, Semin. Cell Dev. Biol. 38 (2015) 16–25.
[6] P. Berndt, L. Winkler, J. Cording, et al., Tight junction proteins at the blood-brain barrier: far more than claudin-5, Cell. Mol. Life Sci. (2019), https://doi.org/10.1007/s00018-019-03030-7, 2019/02/09.
[7] T. Nitta, M. Hata, S. Gotoh, et al., Size-selective loosening of the blood-brain barrier in claudin-5-deficient mice, J. Cell Biol. 161 (2003) 653–660, https://doi.org/10.1083/jcb.200302070.
[8] M. Campbell, A.T. Nguyen, A.S. Kiang, et al., An experimental platform for systemic drug delivery to the retina, Proc. Natl. Acad. Sci. U. S. A. 106 (2009) 17817–17822, 2009/10/14, https://doi.org/10.1073/pnas.0908561106.
[9] C.A. Lipinski, F. Lombardo, B.W. Dominy, et al., Experimental and computational approaches to estimate solubility and permeability in drug discovery and development settings (Reprinted from Advanced Drug Delivery Reviews, vol 23, pg 3-25, 1997), Adv. Drug Deliv. Rev. 46 (2001) 3–26. Reprint, https://doi.org/10.1016/s0169-409x(00)00129-0.
[10] W.M. Pardridge, Molecular biology of the blood-brain barrier, Mol. Biotechnol. 30 (2005) 57–69. Review, https://doi.org/10.1385/mb:30:1:057.
[11] A. Parodi, M. Rudzinska, A.A. Deviatkin, et al., Established and emerging strategies for drug delivery across the blood-brain barrier in brain Cancer, Pharmaceutics 11 (2019), https://doi.org/10.3390/pharmaceutics11050245.
[12] N. Gehne, R.F. Haseloff, I.E. Blasig, Identity crisis in the PMP-22/EMP/MP20/Claudin superfamily (Pfam00822), Tissue Barri. 3 (2015), e1089680, 2015/12/31, https://doi.org/10.1080/21688370.2015.1089680.
[13] H. Suzuki, T. Nishizawa, K. Tani, et al., Crystal structure of a claudin provides insight into the architecture of tight junctions, Science 344 (2014) 304–307, 2014/04/20, https://doi.org/10.1126/science.1248571.
[14] O.R. Colegio, C. Van Itallie, C. Rahner, et al., Claudin extracellular domains determine paracellular charge selectivity and resistance but not tight junction fibril architecture, Am. J. Phys. Cell Phys. 284 (2003) C1346–C1354, 2003/04/18, https://doi.org/10.1152/ajpcell.00547.2002.
[15] C. Piehl, J. Piontek, J. Cording, et al., Participation of the second extracellular loop of claudin-5 in paracellular tightening against ions, small and large molecules, Cell. Mol. Life Sci. 67 (2010) 2131–2140.
[16] G. Krause, L. Winkler, C. Piehl, et al., Structure and function of extracellular claudin domains, Ann. N. Y. Acad. Sci. 1165 (2009) 34–43, 2009/06/23, https://doi.org/10.1111/j.1749-6632.2009.04057.x.
[17] C. Tscheik, I.E. Blasig, L. Winkler, Trends in drug delivery through tissue barriers containing tight junctions, Tissue Barri. 1 (2013), e24565, https://doi.org/10.4161/tisb.24565.
[18] D. Saaber, S. Wollenhaupt, K. Baumann, et al., Recent progress in tight junction modulation for improving bioavailability, Expert Opin Drug Discov 9 (2014) 367–381, 2014/02/25, https://doi.org/10.1517/17460441.2014.892070.
[19] B. Erdlenbruch, V. Jendrossek, H. Eibl, et al., Transient and controllable opening of the blood-brain barrier to cytostatic and antibiotic agents by alkylglycerols in rats, Exp. Brain Res. 135 (2000) 417–422, 2001/01/09, https://doi.org/10.1007/s002210000553.
[20] L. Jena, E. McErlean, H. McCarthy, Delivery across the blood-brain barrier: nanomedicine for glioblastoma multiforme, Drug Deliv. Transl. Res. 10 (2020) 304–318, 2019/11/16, https://doi.org/10.1007/s13346-019-00679-2.
[21] C. Staat, C. Coisne, S. Dabrowski, et al., Mode of action of claudin peptidomimetics in the transient opening of cellular tight junction barriers, Biomaterials 54 (2015) 9–20. Article, https://doi.org/10.1016/j.biomaterials.2015.03.007.
[22] S. Dithmer, C. Staat, C. Muller, et al., Claudin peptidomimetics modulate tissue barriers for enhanced drug delivery, Ann. N. Y. Acad. Sci. 1397 (2017) 169–184. Article, https://doi.org/10.1111/nyas.13359.
[23] A.K. Ghose, V.N. Viswanadhan, J.J. Wendoloski, A knowledge-based approach in designing combinatorial or medicinal chemistry libraries for drug discovery. 1. A qualitative and quantitative characterization of known drug databases, J. Comb. Chem. 1 (1999) 55–68, 2000/04/04.
[24] J. Piontek, S. Fritzsche, J. Cording, et al., Elucidating the principles of the molecular organization of heteropolymeric tight junction strands, Cell. Mol. Life Sci. 68 (2011) 3903–3918.

[25] S. Dabrowski, C. Staat, D. Zwanziger, et al., Redox-sensitive structure and function of the first extracellular loop of the cell-cell contact protein Claudin-1: lessons from molecular structure to animals, Antioxid. Redox Signal. 22 (2015) 1–14.
[26] A. Untergasser, I. Cutcutache, T. Koressaar, et al., Primer3-new capabilities and interfaces, Nucleic Acids Res. (2012) 40. Article, https://doi.org/10.1093/nar/gks596.
[27] G. Del Vecchio, C. Tscheik, K. Tenz, et al., Sodium caprate transiently opens claudin-5-Containing Barriers At Tight Junctions Of Epithelial And Endothelial Cells, Mol. Pharm. 9 (2012) 2523–2533. Article, https://doi.org/10.1021/mp3001414.
[28] M. Allen, M. Bjerke, H. Edlund, et al., Origin of the U87MG glioma cell line: Good news and bad news, Sci. Transl. Med. 8 (2016) 4. Article, https://doi.org/10.1126/scitranslmed.aaf6853.
[29] D. William, C.S. Mullins, B. Schneider, et al., Optimized creation of glioblastoma patient derived xenografts for use in preclinical studies, J. Transl. Med. 15 (2017) 27, 2017/02/12, https://doi.org/10.1186/s12967-017-1128-5.
[30] A. Grosdidier, V. Zoete, O. Michielin, SwissDock, a protein-small molecule docking web service based on EADock DSS, Nucleic Acids Res. 39 (2011) W270–W277. Article, https://doi.org/10.1093/nar/gkr366.
[31] N. Gehne, A. Lamik, M. Lehmann, et al., Cross-over endocytosis of claudins is mediated by interactions via their extracellular loops, PLoS One 12 (2017), e0182106, 2017/08/17, https://doi.org/10.1371/journal.pone.0182106.
[32] J. Piontek, L. Winkler, H. Wolburg, et al., Formation of tight junction: determinants of homophilic interaction between classic claudins, FASEB J. 22 (2008) 146–158. Article, https://doi.org/10.1096/fj.07-8319com.
[33] J. Hou, A.S. Gomes, D.L. Paul, et al., Study of claudin function by RNA interference, J. Biol. Chem. 281 (2006) 36117–36123, https://doi.org/10.1074/jbc.M608853200.
[34] J. Gavard, J.S. Gutkind, VE-cadherin and claudin-5: it takes two to tango, Nat. Cell Biol. 10 (2008) 883–885. Editorial Material, https://doi.org/10.1038/ncb0808-883.
[35] R.S. Beard, R.J. Haines, K.Y. Wu, et al., Non-muscle Mlck is required for beta-catenin- and FoxO1-dependent downregulation of Cldn5 in IL-1 beta-mediated barrier dysfunction in brain endothelial cells, J. Cell Sci. 127 (2014) 1840–1853. Article, https://doi.org/10.1242/jcs.144550.
[36] H.K. Karnati, M. Panigrahi, N.A. Shaik, et al., Down Regulated Expression of Claudin-1 and Claudin-5 and Up Regulation of beta-Catenin: Association with Human Glioma Progression, CNS & Neurol. Disord.-Drug Targets 13 (2014) 1413–1426. Article, https://doi.org/10.2174/1871527313666141023121550.
[37] A. Taddei, C. Giampietro, A. Conti, et al., Endothelial adherens junctions control tight junctions by VE-cadherin-mediated upregulation of claudin-5, Nat. Cell Biol. 10 (2008) 923–934. Article, https://doi.org/10.1038/ncb1752.
[38] M. Vecsernyes, F. Fenyvesi, I. Bacskay, et al., Cyclodextrins, blood-brain barrier, and treatment of neurological diseases, Arch. Med. Res. 45 (2014) 711–729, 2014/12/09, https://doi.org/10.1016/j.arcmed.2014.11.020.
[39] C. Coisne, S. Tilloy, E. Monflier, et al., Cyclodextrins as emerging therapeutic tools in the treatment of cholesterol-associated vascular and neurodegenerative diseases, Molecules 21 (2016), https://doi.org/10.3390/molecules21121748.
[40] D. Lambert, C.A. O'Neill, P.J. Padfield, Depletion of Caco-2 cell cholesterol disrupts barrier function by altering the detergent solubility and distribution of specific tight-junction proteins, Biochem. J. 387 (2005) 553–560, https://doi.org/10.1042/BJ20041377.
[41] V. Kiviniemi, V. Korhonen, J. Kortelainen, et al., Real-time monitoring of human blood-brain barrier disruption, PLoS One (2017) 12. Article, https://doi.org/10.1371/journal.pone.0174072.
[42] N.D. Doolittle, L.L. Muldoon, A.Y. Culp, et al., Delivery of chemotherapeutics across the blood-brain barrier: challenges and advances, Adv. Pharmacol. 71 (2014) 203–243, 2014/10/14, https://doi.org/10.1016/bs.apha.2014.06.002.
[43] K. Heimberger, P. Samec, H. Binder, et al., Blood-brain-barrier disruption interventional neuroradiology in brain-tumor therapy, Ann. Radiol. 29 (1986) 230–232 (Article).
[44] H.L. Liu, M.Y. Hua, P.Y. Chen, et al., Blood-brain barrier disruption with focused ultrasound enhances delivery of chemotherapeutic drugs for glioblastoma treatment, Radiology 255 (2010) 415–425. Article, https://doi.org/10.1148/radiol.10090699.
[45] A. Burgess, C.A. Ayala-Grosso, M. Ganguly, et al., Targeted delivery of neural stem cells to the brain using MRI-guided focused ultrasound to disrupt the blood-brain barrier, PLoS One 6 (2011), e27877, 2011/11/25, https://doi.org/10.1371/journal.pone.0027877.
[46] L.J. Wen, Y.A. Tan, S.H. Dai, et al., VEGF-mediated tight junctions pathological fenestration enhances doxorubicin-loaded glycolipid-like nanoparticles traversing BBB for glioblastoma-targeting therapy, Drug Deliv. 24 (2017) 1843–1855. Article, https://doi.org/10.1080/10717544.2017.1386731.
[47] S.Z. Jiang, R. Xia, Y. Jiang, et al., Vascular endothelial growth factors enhance the permeability of the mouse blood-brain barrier, PLoS One 9 (2014), https://doi.org/10.1371/journal.pone.0086407.
[48] M. Campbell, A.S. Kiang, P.F. Kenna, et al., RNAi-mediated reversible opening of the blood-brain barrier, J. Gene Med. 10 (2008) 930–947. Article, https://doi.org/10.1002/jgm.1211.
[49] M. Campbell, M.M. Humphries, A.S. Kiang, et al., Systemic low-molecular weight drug delivery to pre-selected neuronal regions, Embo Mol. Med. 3 (2011) 235–245. Article, https://doi.org/10.1002/emmm.201100126.
[50] Y. Hashimoto, K. Shirakura, Y. Okada, et al., Claudin-5-Binders Enhance Permeation of Solutes across the Blood-Brain Barrier in a Mammalian Model, J. Pharmacol. Exper. Therap. 363 (2017) 275–283. Article, https://doi.org/10.1124/jpet.117.243014.
[51] S.M. Hedrick, R.H. Michelini, A.L. Doedens, et al., FOXO transcription factors throughout T cell biology, Nat. Rev. Immunol. 12 (2012) 649–661. Review, https://doi.org/10.1038/nri3278.
[52] B.W. Doble, J.R. Woodgett, GSK-3: tricks of the trade for a multi-tasking kinase, J. Cell Sci. 116 (2003) 1175–1186. Review, https://doi.org/10.1242/jcs.00384.
[53] J.J. Heimans, J.B. Vermorken, J.G. Wolbers, et al., Paclitaxel (Taxol(R)) concentrations in brain-tumor tissue, Ann. Oncol. 5 (1994) 951–953. Note, https://doi.org/10.1093/oxfordjournals.annonc.a058736.
[54] A.S. Mohammad, C.E. Adkins, N. Shah, et al., Permeability changes and effect of chemotherapy in brain adjacent to tumor in an experimental model of metastatic brain tumor from breast cancer, BMC Cancer 18 (2018) 1225, 2018/12/12, https://doi.org/10.1186/s12885-018-5115-x.